Investigation of the Heterogeneous Reactivity of HCl, HBr, and HI on Ice Surfaces

Stephen B. Barone

Department of Chemistry, George Washington University, Washington, DC 20052

Mark A. Zondlo and Margaret A. Tolbert*

Department of Chemistry and Biochemistry and Cooperative Institute for Research in Environmental Sciences, University of Colorado, Boulder, Colorado 80309

Received: February 3, 1999; In Final Form: August 6, 1999

The interactions of hydrogen halide gases (HX = HCl, HBr, and HI) with thin ice films representative of atmospheric aerosols have been studied using a Knudsen cell reactor coupled to a Fourier transform infrared−reflection absorption (FTIR−RAS) spectroscopic probe. The gas-phase uptake and reaction products resulting from the exposure of hydrogen halides to ice surfaces over a wide range of temperatures (110−210 K), hydrogen halide partial pressures ($5-1000 \times 10^{-7}$ Torr), and ice film thicknesses (10−100 nm) are reported. Studies of HCl and HBr showed efficient reactions on crystalline and amorphous microporous ice films at 110 K to form H_3O^+ until reaching coverages ranging from $(5-20) \times 10^{15}$ molecules cm^{-2}, after which the rate of reaction dramatically decreased. The uptake of HCl on hexagonal crystalline ice at temperatures representative of the lower stratosphere and upper troposphere (180−210 K) was found to depend strongly on HCl partial pressure. Over the temperature range studied, exposure of ice to HCl partial pressures below the HCl equilibrium partial pressure at the liquid/ice coexistence point resulted in uptake limited to $(3.5 \pm 1.6) \times 10^{15}$ molecules cm^{-2}. In contrast, exposure to HCl pressures larger than the HCl equilibrium partial pressure resulted in unlimited uptake. HBr and HI were efficiently and continuously taken up by ice surfaces ($\gamma \geq 0.02$) over a range of atmospherically relevant temperatures (180−210 K). Although crystalline hydrates of $HX:H_2O$ are stable over the temperature range examined, the incorporation of hydrogen halides into ice always resulted in the formation of amorphous $HX:H_2O$ product layers with the exception of HBr uptake at high flow rates (flow rate $\geq 3.1 \times 10^{15}$ molecules s^{-1}) which resulted in the formation of a mixture of crystalline hydrates.

Introduction

Since the first report of the Antarctic ozone hole in 1985,[1] extensive measurements in the laboratory and field have clearly demonstrated that heterogeneous reactions are important in controlling the abundance of O_3 in the polar stratosphere and at mid-latitudes.[2−5] Heterogeneous reactions occurring on the surfaces of polar stratospheric clouds (PSCs) and sulfate aerosols convert halogen reservoirs into photochemically labile forms which comprise an important photolytic source of halogen radicals in the lower stratosphere. For example, the following reaction:

$$ClONO_{2(g)} + HCl_{(s)} \rightarrow Cl_{2(g)} + HNO_{3(s)} \qquad (1)$$

provides an efficient pathway to convert relatively stable forms of atmospheric chlorine ($ClONO_2$ and HCl) to Cl_2 which photolyzes rapidly to produce Cl radicals. In addition to directly affecting the speciation of stratospheric chlorine, reaction 1 also sequesters NO_x (≡ NO and NO_2) by converting $ClONO_2$ to HNO_3. In turn, the loss of NO_x lowers the rate of chlorine reservoir formation via reaction 2:

$$ClO_{(g)} + NO_{2(g)} \rightarrow ClONO_{2(g)} \qquad (2)$$

Although less abundant and possessing shorter atmospheric lifetimes, bromine reservoirs such as $BrONO_2$, HOBr, and HBr have also been suggested to participate in important heterogeneous chemistry on stratospheric aerosols. The hydrolysis of $BrONO_2$ leads to the production of HOBr via reaction 3:

$$BrONO_{2(g)} + H_2O_{(s)} \rightarrow HOBr_{(g)} + HNO_{3(s)} \qquad (3)$$

Upon release to the gas phase, HOBr is rapidly photolyzed to form OH and Br radicals which can influence the abundance of O_3 in the lower stratosphere.[6−8]

Although less well understood, heterogeneous reactions of halogen reservoirs on ice surfaces are also likely to be important in regulating ozone levels in the troposphere. The upper troposphere is characterized by a large number of ice particles in cirrus clouds and airplane condensation trails that provide ample surfaces for important heterogeneous chemistry.[9,10] Indeed, field observations have shown large decreases of ozone within cirrus clouds supporting a possible role for heterogeneous halogen chemistry in the upper troposphere.[11] Recently, Borrmann et al.[12] and Solomon et al. [13] showed that the inclusion of heterogeneous chlorine chemistry on cirrus cloud surfaces greatly influences the ozone mixing ratios in the upper troposphere. Filterable bromine species have also been implicated in the annual springtime destruction of O_3 in the Arctic boundary layer. The observed O_3 loss has been suggested to involve bromine activation via chemical reactions occurring on aerosol and snow ice surfaces.[14−16]

Previous studies of the heterogeneous chemistry of HCl have focused on quantifying the rates of its reactions with a variety

* Corresponding author. E-mail: tolbert@colorado.edu.

10.1021/jp990400c CCC: $18.00
Published on Web 11/04/1999

of model aerosol surfaces. Due to the widely recognized importance of type II PSCs in the ozone chemistry of the polar stratosphere, the interaction of HCl with crystalline water ice is well characterized from 180 to 200 K and previous studies have shown a strong dependence on HCl partial pressure. At low partial pressures of HCl, uptake on crystalline water ice is limited to approximately 0.4−16 monolayers ($\approx(5-180) \times 10^{14}$ molecules cm^{-2}), while at high HCl partial pressures continuous and efficient uptake ($\gamma > 0.2$) is observed.[17−20]

The heterogeneous reactions of bromine and iodine reservoirs have been much less thoroughly investigated. The available laboratory data suggest that HBr uptake on crystalline ice is independent of HBr partial pressure and very efficient ($\gamma > 0.2$).[16,21,22] The reactivity of HI on surfaces representative of atmospheric aerosol is currently not well understood. However, recently Chu and Chu reported that HI is also efficiently taken up by ice surfaces at stratospheric temperatures.[23]

While there have been several studies of the uptake of hydrogen halides on ice surfaces under stratospheric conditions, very little is known about the reactivity of ice under conditions representative of the troposphere. The troposphere is characterized by large ice surface area densities (20−20000 $\mu m^2\ cm^{-3}$),[24] high temperatures (210−250 K), and low hydrogen halide concentrations. Considering that ice particles in the troposphere possess greater surface area densities than that of the stratosphere and are present globally, laboratory investigations of the reactivity of ice over the entire range of temperatures encountered throughout the troposphere are greatly needed.

In the present study the reactivities of a variety of hydrogen halides (HCl, HBr, and HI) with thin water ice films have been investigated over a wide range of temperatures (110−210 K) and hydrogen halide pressures ($5-1000 \times 10^{-7}$ Torr):

$$\mathrm{HCl} + \mathrm{ice} \rightarrow \mathrm{products} \quad (4)$$

$$\mathrm{HBr} + \mathrm{ice} \rightarrow \mathrm{products} \quad (5)$$

$$\mathrm{HI} + \mathrm{ice} \rightarrow \mathrm{products} \quad (6)$$

Our experimental approach combines kinetic measurements of the heterogeneous reaction efficiency with simultaneous monitoring of the condensed-phase surface and bulk during the course of reaction. In this way we hope to understand the gas-phase kinetics observed in the context of changes occurring on the reactant surface. In addition, this approach allows for the direct observation of the condensed-phase reaction products expected to form in the atmosphere.

Experimental Section

The uptake of HCl, HBr, and HI on thin crystalline and amorphous microporous water ice films was studied using a Knudsen cell flow reactor equipped for grazing angle incidence Fourier transform infrared spectroscopy, a highly sensitive surface/bulk probe. The apparatus used in these studies has been described in detail previously,[25−28] thus, we only mention the aspects necessary to understand the current work.

The apparatus consists of two stainless steel chambers connected by a butterfly valve as shown schematically in Figure 1. The upper chamber houses a circular, optically-flat aluminum substrate (diameter = 9.14 cm, thickness = 0.22 cm) onto which thin water ice films are deposited. The substrate is cooled and heated from the backside by a temperature-controlled cryostat. A differentially pumped sleeve houses the entire heating/cooling assembly to ensure that the only cold surface in the chamber is the thin aluminum substrate.

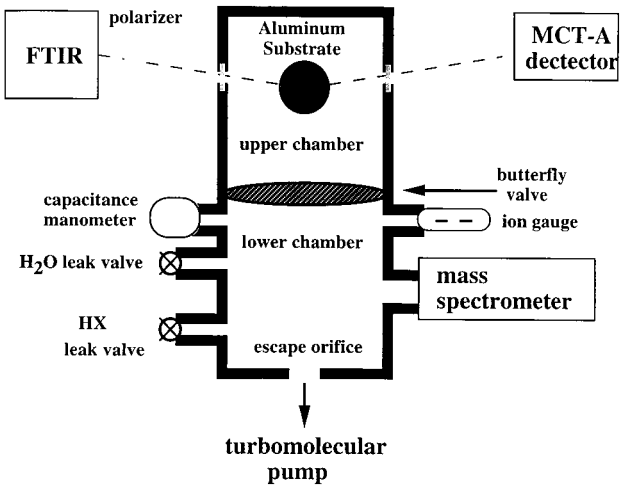

Figure 1. FTIR−RAS/Knudsen reactor used in present study. See text for relevant experimental dimensions.

The temperature of the aluminum substrate is measured by three copper−constantan thermocouples glued directly onto the substrate surface using a thermally conductive epoxy. The surface temperature is also indirectly monitored by relating the measured frost point vapor pressure of H_2O over the ice film to the frost point temperature using the vapor pressures reported by Marti and Mauersberger.[29] The thermocouple temperature measurements always agreed within ±2 K of the experimentally measured frost point temperature. Our cryostat configuration allows for accurate temperature control over the range of 90−400 K with a stability of ≤0.2 K. The temperature gradient across the substrate was 0.5 at 185 K, as measured by thermocouples glued to across the entire 9.14 cm diameter surface. The coldest point of the surface was in the center, and a slight warming occurred toward the edge of the disk.

The lower chamber is coupled to a differentially pumped electron-impact ionization mass spectrometer, an ionization gauge, and a Baratron capacitance manometer to measure gas-phase partial pressures. H_2O, HCl, HBr, and HI were introduced into the lower chamber through separate leak valves. The chamber is pumped through a 64 cm^2 gate valve upstream of a turbomolecular pump. For determination of reaction efficiencies the gate valve was closed so that pumping occurred effusively through a 0.17 cm^2 orifice drilled into the gate valve.

Determination of Reaction Efficiency. The reaction efficiency, γ, is defined as the fraction of collisions with a surface that leads to loss of gas-phase species:

$$\gamma = (\text{no. of molecules lost to surface})/(\text{no. of gas−surface collisions}) \quad \text{(I)}$$

The reaction efficiencies of HCl, HBr, and HI on water ice surfaces were determined by measuring the first-order loss rates resulting from uptake to the surface relative to the loss rate via effusion through the pump-out hole. The loss rate via effusion can be calculated for conditions of molecular flow, hence, absolute reaction efficiencies were obtained.

To obtain reaction efficiencies the following methodology was used. After preparing a reactant ice film in equilibrium with water vapor, the butterfly valve between the two chambers was closed. Next, a hydrogen halide flow was introduced into the lower chamber and monitored by the mass spectrometer. Under these conditions, the only loss mechanism of the gas was via effusion through the small orifice up-stream of the turbomolecular pump. After attaining a steady flow, the butterfly valve

between the upper and lower chambers was opened. If reaction with the ice film surface constitutes a loss mechanism of a rate comparable to that of the loss via effusion, a decrease in the steady-state partial pressure of reactant gas is expected. Assuming the gases are well mixed, the reaction efficiency can be related to the steady-state concentrations before and after exposure to the reactant surface:

$$\gamma = \frac{A_h}{A_s}\left[\frac{[HX]_{ss1} - [HX]_{ss2}}{[HX]_{ss2}}\right] = \frac{A_h}{A_s}\left[\frac{I_0 - I}{I}\right] \quad \text{(II)}$$

where A_h and A_s are the areas of the hole and the surface, respectively, and I_0 and I are the mass spectrometer signals before and after exposing the gas to the reaction surface.[26]

As shown in eq II, to obtain absolute measurements of reaction efficiency the effective area of the escape orifice must be accurately known. The effective area is slightly smaller than the geometric area because the hole is actually a cylinder rather than a perfect disk. The effective hole area ($A_h = 0.17 \pm 0.01$ cm^2) was experimentally determined as described by Barone et al.[26]

The uptake of HCl, HBr, and HI by the stainless steel walls of the chamber in the absence of a reactant ice film was unavoidable. To characterize the deposition to the chamber walls, hydrogen halide flows ranging $(150-1.5) \times 10^{14}$ molecules s^{-1} were expanded into the upper chamber in the absence of ice while directly monitoring the HX concentration by mass spectroscopy. The temporal profiles obtained were characterized by a decrease in signal followed by a recovery within 1 min to a value slightly below that prior to expansion. Within experimental uncertainties, the observed recoveries for HCl, HBr, and HI were identical. This behavior indicates that the stainless steel walls of the chamber acted as a small but continuous sink for gas-phase HCl, HBr, and HI. Therefore, all reaction efficiencies and surface coverages reported in the present work were corrected for the deposition of hydrogen halides on to the walls of the chamber by subtracting out the loss of hydrogen halides observed in the absence of a reactant ice film. The correction associated with wall losses ranged from 3 to 50% of the mass spectrometer signals (I) used in calculating reaction efficiencies using equation II. In addition, the subtraction correction ranged from 10 to 45% of the total integrated areas used in the calculation of the surface coverages reported. Therefore, the background wall loss correction served as the primary source of uncertainty when measuring small reaction efficiencies and small surface coverages and are reflected in the error bars reported.

Condensed-Phase Detection. Characterization of the composition and phase of the reactant ice films and condensed-phase products was performed in situ by Fourier transform infrared reflection absorption spectroscopy (FTIR−RAS) at a grazing angle. Briefly, light from a Nicolet 550 Magna FTIR spectrometer was passed through a Molectron wire-grid polarizer to select only light polarized parallel to the plane of incidence of the reflected light. The light was then focused by a parabolic mirror onto the metal substrate at a near grazing angle of incidence (≈84° from the surface normal). The reflected beam was collected by an ellipsoidal mirror and focused onto a liquid nitrogen cooled HgCdTe-A detector. Typically, infrared spectra were collected over the range of 4000−650 cm^{-1} at 3 s intervals and consisted of the co-addition of 64 interferograms obtained at a resolution of 16 cm^{-1}.

Film thickness measurements of the reactant ice films were determined using optical interference methods. In this technique a HeNe laser ($\lambda = 632.8$ nm) beam was reflected off the metal surface at 23° from the surface normal and detected by a photodiode. Film thickness was experimentally determined by monitoring the beam intensity while an ice film was grown at a constant deposition velocity. Reflection occurs at both the gas−film and film−substrate interfaces. Therefore, as the film grows, the two reflected beams interfere to produce a sinusoidal interference pattern. The film thickness as a function of growth time can be extracted from eq III:

$$\text{thickness} = \frac{m\lambda}{2n(T)\cos\phi} \quad \text{(III)}$$

where $n(T)$ is the temperature-dependent refractive index, m is the period of oscillation, λ is the wavelength of the impinging beam, and ϕ is the angle of refraction. The solution of eq III for a growing ice film on aluminum at 165 K yields a thickness of 252 nm at one constructive interference fringe.

The FTIR−RAS spectra of growing ice films also yields information pertaining to film thickness. To gain a quantitative understanding of the relationship between total integrated absorbance and film thickness, optical interference measurements were made simultaneously with the collection of FTIR−RAS spectra of growing ice films. The total integrated absorbance of the OH stretch (3800−2850 cm^{-1}) varied linearly with film thickness for thickness <100 nm. Plotting the total integrated absorbance of the OH stretching vibration (2850−3800 cm^{-1}) versus ice thickness determined by optical interference yielded a straight line described by eq IV:

$$I(2850-3800\ \text{cm}^{-1}) = (2.08 \pm 1.48) \times t - 1.48 \quad \text{(IV)}$$

where I is the total integrated absorbance and t is the thickness in nanometers. Therefore, in experiments investigating the uptake of hydrogen halides onto thin ice films, the thickness of the reactant ice films was directly inferred from the observed FTIR−RAS spectra prior to reaction using eq IV.

In addition to determining reactant film thickness, FTIR−RAS yields information pertaining to the phase and composition of condensed-phase products formed during reactions 4−6. To aid in characterizing the condensed-phase spectra of the growing product layers, reference spectra of amorphous and crystalline H_2O/HX mixtures were acquired. Reference spectra of amorphous H_2O:HX mixtures were determined by introducing flows of H_2O and HX into the lower chamber corresponding to a variety of stoichiometric partial pressures. Upon attaining stable flows, the butterfly valve was opened and the gas flows were placed in contact with the aluminum substrate held at 140 K. Assuming unity sticking coefficients of HX and H_2O on the resulting HX/H_2O amorphous mixtures, FTIR−RAS reference spectra were obtained for HCl, HBr, and HI mixtures over a range of H_2O:HX stoichiometric ratios. Within experimental uncertainty, the reference spectra obtained for each hydrogen halide were identical for a given amount of water. As an example, Figure 2A shows the H_2O:HBr reference spectra obtained for stoichiometric ratios of 2:1, 3:1, 4:1, and 6:1, H_2O and HBr, respectively. To further characterize these reference spectra, the relative intensities of the OH stretch (3400 cm^{-1}) to the ν_4 asymmetric bending mode of H_3O^+ (1750 cm^{-1}) were quantified over a baseline drawn from 3800 to 1070 cm^{-1}. Peak ratios of 2.5, 3.3, 4.4, and 7.0 for OH/H_3O^+ were determined for film compositions of 2:1, 3:1, 4:1, and 6:1, H_2O and HBr,

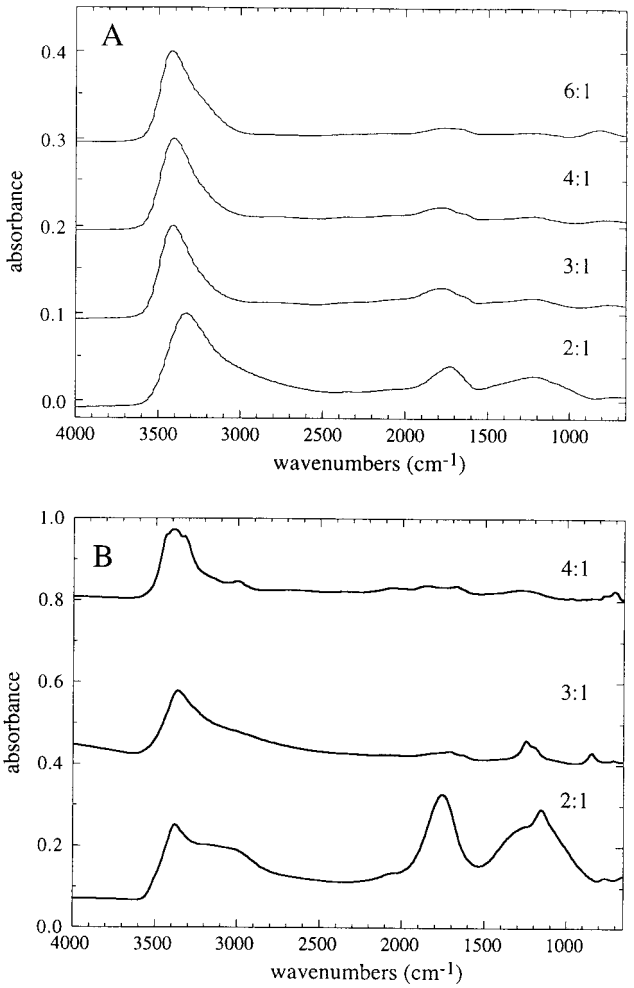

Figure 2. Reference spectra of amorphous and crystalline H_2O:HBr mixtures. Panel A shows amorphous films at 140 K for a variety of H_2O and HBr stoichiometeric ratios (indicated on plot). Panel B shows several crystalline hydrates of H_2O:HBr obtained via vapor deposition at 110 K followed by annealing to 160 K at a rate of 10 K min^{-1}.

TABLE 1: Peak Positions (cm^{-1}) of Thin HX and Amorphous HX/H_2O Films

			H_2O:HBr			
HCl	HBr	HI	2:1	3:1	4:1	6:1
2758	2435	2137	720	748	770	810
2715	2425		1220	1220	1220	1220
			1694	1730	1770	1750
			3330	3400	3400	3420

respectively. The peak positions for the reference spectra obtained are summarized in Table 1. It should be noted that the peak positions measured in the present study varied slightly (± 20 cm^{-1}) with film thickness. This dependence has been observed in other studies utilizing reflection absorption at a grazing incidence.[25] Therefore, reported peak positions can be considered to have an uncertainty of ± 20 cm^{-1}. Although the spectra in Figure 2 agree reasonably well with the results of previous studies, several differences are noted. In particular, Delzeit et al. report transmission spectra of a 2:1 H_2O:HBr film which includes a peak at 2220 cm^{-1}. The reason for this discrepancy is unknown but may be related to differences between reflection absorption and transmission spectroscopic techniques.

Reference spectra of crystalline HX:H_2O films were also determined for a number of stoichiometric ratios. To prepare crystalline reference spectra, amorphous mixtures of H_2O and HX with a well-defined stoichiometry were deposited at 110 K and annealed to 160 K at a rate of 10 K min^{-1}. Typically, crystallization was observed at $T \geq 150$ K and was characterized by the appearance of sharp absorption features and the occurrence of strong light extinction due to scattering at frequencies ≥ 2500 cm^{-1}. The sensitivity to light scattering upon crystallization is likely due to the large angle of incidence used in the present study. Slight changes in the composition of the film were also noticed during annealing and were unavoidable. As an example, reference spectra of crystalline H_2O:HBr mixtures of stoichiometry 2:1, 3:1 and 4:1 H_2O:HBr are summarized in Figure 2B.

Reagents. HCl (Matheson, >99.0%) and H_2O (Aldrich, HPLC grade) were used without further purification and were introduced to the chamber via glass inlet lines. HBr (Matheson, >99.8%) and HI (Matheson, >98%) required purification prior to use because they degrade significantly in stainless steel lecture bottles to form H_2, Br_2 and I_2. HBr and HI were purified on-line by freezing a several milliliter aliquot in a liquid nitrogen trap and pumping to remove any H_2 in the sample. The frozen samples appeared as white crystals with very little color from Br_2 or I_2 impurities (which show up as brown and yellow crystals, respectively). Once purified, the HBr and HI samples were warmed and expanded into glass inlet lines for introduction into the apparatus. After use, the gaseous HBr and HI samples were easily recondensed and showed no visual sign of further degradation in the glass inlets.

The mass spectrometer fragment signals from HCl (m/z = 35, 36, 37, 38), HBr (m/z = 79, 80, 81, and 82) and HI (m/z = 127 and 128) were linear with respect to partial pressure over the range $(5-1000) \times 10^{-7}$ Torr. H_2O was monitored mass spectrometerically using mass peak m/z = 18 and also determined directly from the capacitance manometer located in the chamber.

Results

HX Deposition on Aluminum at 94 K. To quantitatively assess the purity of our gas samples as well as to characterize the FTIR−RAS spectra of the molecular (nondissociated) forms of HCl, HBr, and HI, solid hydrogen halide films were prepared by vapor deposition on to the aluminum substrate at 94 K. Figure 3 shows three infrared spectra obtained by exposing the aluminum surface to partial pressures of HCl, HBr, and HI of 3.0×10^{-4}, 1.8×10^{-4}, and 1.0×10^{-4} Torr, respectively. The base partial pressure of H_2O in our chamber ($\approx 2 \times 10^{-8}$ Torr) is sufficiently high that condensation of a small amount of H_2O is unavoidable at 94 K. Therefore, the spectra in Figure 3 represent the various hydrogen halides deposited on ≤ 2 nm thick water ice films. Figure 3 show the fundamental absorptions for thin (<100 nm) films of HCl (2758 cm^{-1} and 2715 cm^{-1}), HBr (2435 and 2425 cm^{-1}) and HI (2137 cm^{-1}). The line positions observed are in good agreement with similar transmission and reflection absorption spectra in the literature.[30,31] No other absorptions were observable over the entire mid infrared range of our detector (4000−650 cm^{-1}), suggesting our hydrogen halide samples were free from impurities that absorb in the mid infrared. Following vapor deposition of the hydrogen halides, the temperature was increased at a rate of 10 K min^{-1} and the hydrogen halide films rapidly desorbed. HCl desorbed at 100 K while HBr and HI films desorbed at slightly higher temperatures of 107 and 120 K, respectively.

Deposition of HX on Ice at 110 K. The uptake of HCl and HBr on thin ice films was first investigated at 110 K. We report measurements of uptake on both crystalline and amorphous microporous ice films over a range of ice thicknesses (10−100

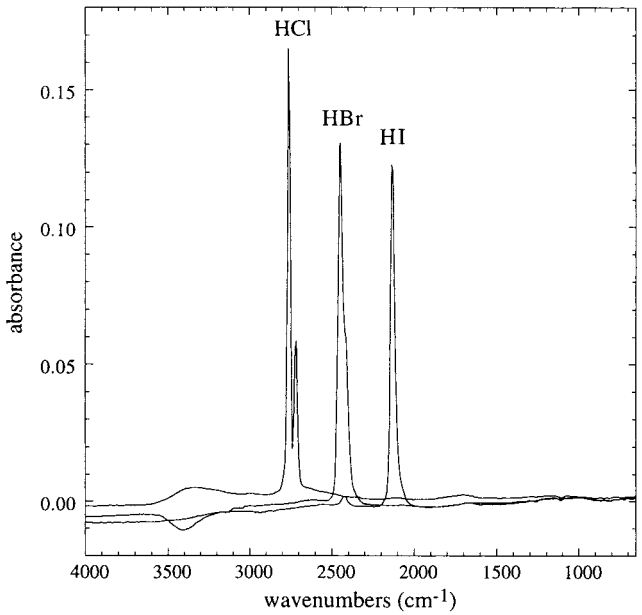

Figure 3. FTIR−RAS spectra of condensed films of HCl (2758 cm^{-1}), HBr (2435 cm^{-1}), and HI (2137 cm^{-1}) at 94 K. Partial pressures and exposure times are $P(HCl) = 3.0 \times 10^{-4}$ Torr for 9.1 s, $P(HBr) = 1.8 \times 10^{-4}$ Torr for 13.7 s, and $P(HI) = 1 \times 10^{-4}$ Torr for 54.8 s. The slight absorptions, negative and positive, at 3400 cm^{-1} are related to amorphous ice formation prior to exposure to the HX sample. Background spectra taken before cooling lead to positive values of absorbance at 3400 cm^{-1}, while background spectra taken immediately prior to deposition at 94 K lead to negative values of absorbance at 3400 cm^{-1}.

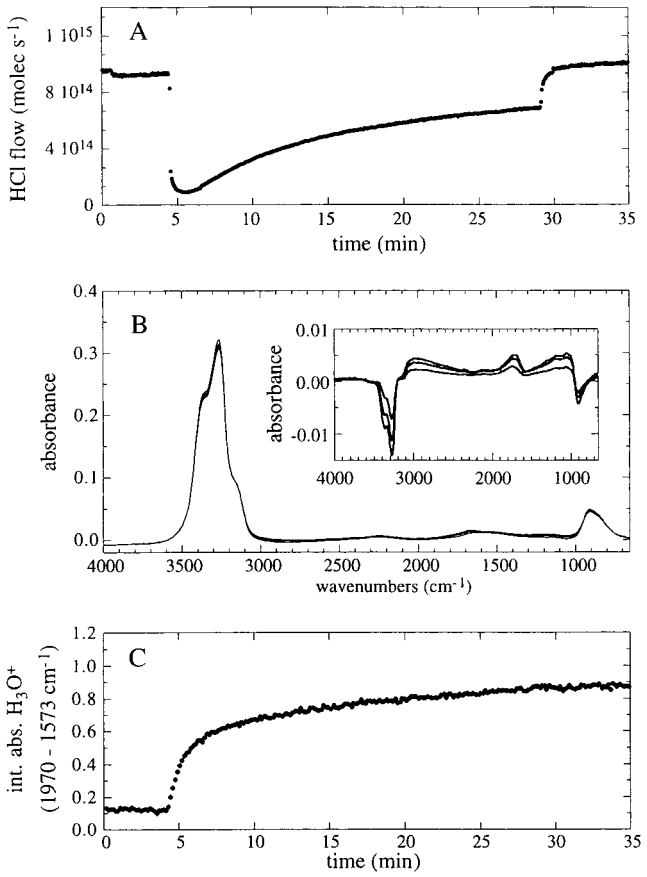

Figure 4. Infrared spectra and mass spectrometer temporal profiles obtained upon exposure of a HCl flow (flow rate = 9.3×10^{14} molecules s^{-1}) to a 33 nm thick crystalline ice film at 110 K. Panel A shows the temporal behavior of gas-phase HCl ($m/z = 36$) observed by the mass spectrometer prior to and during deposition. Panel B shows the FTIR−RAS spectra acquired at $t = 0$, 1.4, 2.6, and 5.2 min after opening the butterfly valve. The inset in panel B shows the subtraction spectra acquired at the times given above. Panel C shows the integrated absorbance of the H_3O^+ peak (1970−1573 cm^{-1}) as a function of exposure time before and during exposure.

nm). Crystalline ice films were formed by vapor deposition of H_2O at 140 K followed by annealing to 160 K at a rate of 10 K min^{-1}. A significant change in the infrared spectra of the annealing ice films was noted at temperatures above ≈150 K, indicating an ordering of amorphous ice to a crystalline lattice. Amorphous microporous ice films were formed by vapor deposition of H_2O on the aluminum substrate at 110 K. The spectra of amorphous microporous ice showed a small but significant absorption at 3695 cm^{-1}, indicating the presence of free OH groups on the surface and within the micropores of the ice films. The infrared spectra for the crystalline and amorphous microporous ice films investigated in the present work are in excellent agreement with previous FTIR studies.[25,32,33]

Upon obtaining a crystalline or amorphous microporous ice film of the desired thickness (10−100 nm) at 110 K, the butterfly valve separating lower and upper chambers was closed. Next, a flow of HCl or HBr in the range $(5-20) \times 10^{14}$ molecules s^{-1} was introduced to the lower chamber. The butterfly valve was opened after attaining a stable flow, and the reactant ice film was exposed to a flow of hydrogen halide gas. As examples, Figures 4A and 5A show the $m/z = 36$ (HCl) signals observed upon exposing HCl to crystalline and amorphous microporous ice films, of thickness 33 and 34 nm, respectively. Large decreases were observed in the mass spectrometer signals immediately after opening the butterfly valve. The decreases observed in the mass spectrometer signals were followed by a recovery at longer exposure times. Eventually, the HCl signals leveled off to a value slightly below that observed prior to exposure. Using eq II the mass spectrometer signals yield an initial value of $\gamma \geq 0.02$ and a value of $\gamma \leq 0.0004$ for HCl uptake at long exposure times (post recovery) for reaction 4 on crystalline and amorphous microporous ice films. This behavior indicates an efficient uptake of hydrogen halides at short reaction times followed by a saturation of reactive surface sites at long exposure times. The uptake of HCl was studied on ice films ranging from 10 to 100 nm in thickness. In each case similar temporal behavior was observed. Exposure of HBr to crystalline and microporous ice films also yielded similar temporal profiles characterized by a dramatic decrease in signal followed by recovery at longer times.

Although similar in shape, a comparison of the temporal behavior of the mass spectrometer signals following exposure of hydrogen halides to amorphous microporous and crystalline ice films shows quantitative differences. Specifically, in experiments exposing identical halogen flow rates to crystalline and amorphous microporous ice, mass spectrometer signals recovered at later times for exposure to amorphous microporous ice. This behavior suggests that amorphous microporous ice exhibits a net enhanced reactivity toward hydrogen halide gases over crystalline ice.

Infrared spectra were acquired simultaneously during exposure of the microporous and crystalline ice films to hydrogen halide flows. The reactant film spectra exhibited significant changes within the first few minutes of exposure followed by slight changes at longer times. The ice spectra exhibited identical changes for deposition of both hydrogen halides investigated. As an example, the spectra acquired upon exposure of an HCl flow of 9.3×10^{14} molecules s^{-1} to a 33 nm thick crystalline ice film are shown in Figure 4B. To highlight the changes that

occurred upon exposure, subtraction spectra for times $t = 1.4$, 2.6, and 5.2 min after exposure are shown as an inset in Figure 4B. A decrease in absorbance at the frequencies corresponding to the OH stretch (3260 cm^{-1}) and libration (850 cm^{-1}) of the crystalline ice spectra occurred simultaneously with the appearance and growth of a broad absorption feature centered at 1750 cm^{-1}. This new absorption may be assigned to the ν_4 antisymmetric bending vibration in H_3O^+ formed at the ice interface.[30,31,34,35] The observed changes clearly indicate that H_3O^+ is formed by the dissociation of the adsorbed H−X species and subsequent reaction with H_2O. Figure 4C shows the temporal evolution of the H_3O^+ absorption band at 1750 cm^{-1} prior to and during exposure. As shown in Figure 4C, opening the butterfly valve initiated a rapid increase in the rate of formation of H_3O^+ on the reactant ice film. However, after approximately 10 min the formation rate of H_3O^+ slowed considerably and eventually became small. The temporal profile of H_3O^+ shows a time dependence strikingly similar to that observed in the gas-phase loss rate (Figure 4A). Specifically, the growth rate of H_3O^+ decreases at the same time as the gas-phase loss rate decreases. Although the reaction rate dramatically decreased at long times, exposure for extended times (>60 min) resulted in the complete reaction of the reactant ice film for the thinnest ice films investigated.

The spectra of amorphous microporous ice exhibited similar changes upon exposure to HCl and HBr gas flows. Figure 5B shows spectra taken before and during exposure of a HCl flow of 8.8×10^{14} molecules s^{-1} to a 34 nm amorphous microporous ice film. As shown in Figure 5B, HCl exposure to amorphous microporous ice films also resulted in the appearance and growth of a broad absorption-centered at 1750 cm^{-1} attributable to H_3O^+ production. The temporal profile of the 1750 cm^{-1} band (H_3O^+) is presented in Figure 5C and is characterized by a rapid rate of formation upon exposure followed by a rapid decrease in the H_3O^+ formation rate at $t \approx 20$ min. Although it cannot be easily observed on the scale of the insert in Figure 5B, an immediate decrease in the absorption assigned to the free OH stretch (3695 cm^{-1}) in our amorphous microporous ice films was also observed upon exposure to HCl and HBr. It is clear that immediately after exposure all of the free OH bonds observable have reacted away.

No significant absorption was observed at the frequencies corresponding to the molecular stretch for molecular HCl and HBr (2758 and 2435 cm^{-1}) upon exposure of an HX flow to either crystalline or amorphous microporous ice at 110 K. This suggests that the majority of the impinging HX molecules ionize upon incorporation to the reactant ice film, regardless of the phase of the reactant ice film.

HCl on Ice at 185−210 K. The uptake of HCl on hexagonal crystalline water ice was investigated as a function of HCl partial pressure over a range of stratospherically and tropospherically relevant temperatures. In these experiments thin (10−100 nm) hexagonal crystalline ice films were prepared by flowing H_2O into the upper chamber to achieve nucleation at $T = (185-210$ K). After achieving the desired film thickness, the water partial pressure was adjusted so that no change in the infrared spectra of the film was noticeable over a 5 min interval. At temperatures greater than 190 K, the FTIR−RAS spectra of the reactant ice film exhibited light extinction from scattering in addition to the characteristic crystalline water ice absorption. This is likely due to surface roughening attributable to the highly dynamic nature of ice above 190 K.[36]

Figure 6A shows the $m/z = 36$ temporal profile obtained upon exposing a HCl flow (flow rate = 3.5×10^{14} molecules s^{-1}) to a 51 nm ice film at 202 K. Upon opening the butterfly valve at $t = 6.3$ min, a dramatic decrease in the $m/z = 36$ signal was observed followed by a slow recovery over the next ≈40 min. After closing the butterfly valve at $t = 55$ min the mass spectrometer signals rapidly recovered to their original values. Upon opening the butterfly valve a second time a slight drop was observed to the value prior to closing the butterfly valve for the first time and the slow recovery was observed to continue. The mass spectrometer signals before (I_o) and after (I) opening the butterfly valve are related to the reaction efficiency for reaction 4 via eq II. The mass spectrometer signals $m/z = 35$ and $m/z = 36$ yielded an average value of $\gamma = 0.005$ immediately after opening the butterfly valve. After approximately 50 min the reaction efficiency had decreased to a value of $\gamma = 0.0005$.

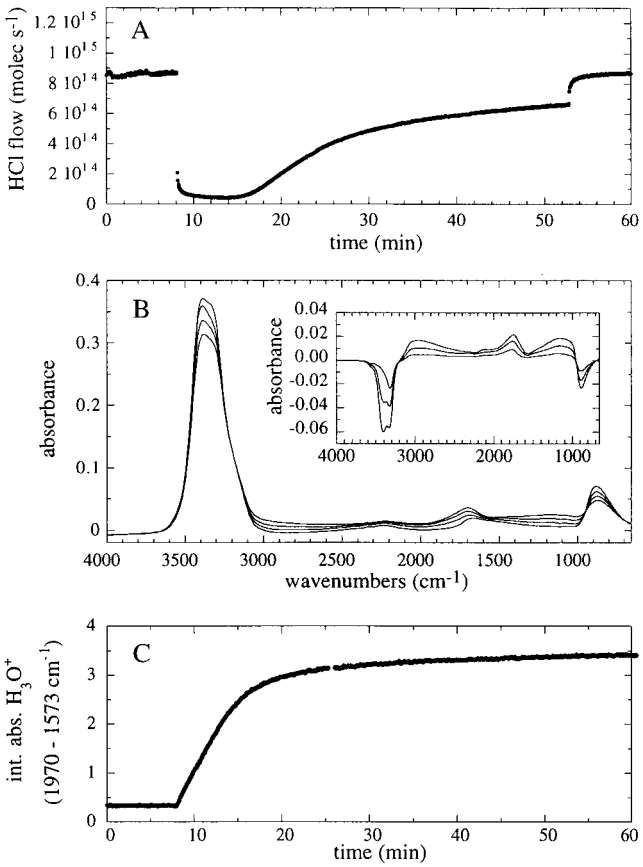

Figure 5. Infrared spectra and mass spectrometer temporal profiles resulting from the exposure of a HCl flow (flow rate = 8.8×10^{14} molecules s^{-1}) to a 34 nm thick amorphous microporous ice film at 110 K. Panel A shows the temporal behavior observed by the mass spectrometer prior to and during deposition of HCl ($m/z = 36$). Panel B shows the FTIR−RAS spectra acquired at $t = 0$, 2.9, 5.9, and 12 min after opening the butterfly valve. The inset in panel B shows the subtraction spectra acquired at the times given above. Panel C presents the temporal evolution of the H_3O^+ product peak (1970−1573 cm^{-1}) observed during exposure.

The spectra of the reactant ice film exhibited very few changes throughout the entire ≈60 min of exposure time. Figure 6B shows the spectra of the reactant ice film at several time intervals. The most significant change observed in the infrared spectrum of the reactant ice film was an increase in light extinction at $\nu > 3600$ cm^{-1}. This behavior is indicative of an increase in the extent of light scattering from the thin film and is presumably due to an increase in the film roughness. Subtraction spectra (not shown) at a number of different time intervals reveal a slight increase in the extinction at ≈1750 cm^{-1}

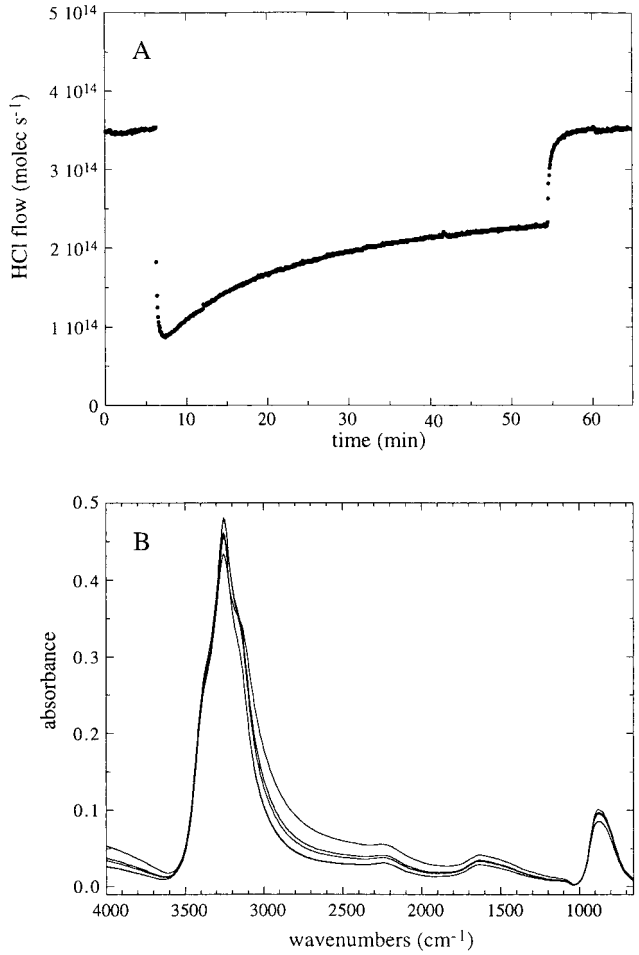

Figure 6. Infrared spectra and mass spectrometer temporal profiles obtained upon the exposure of a low HCl flow rate (flow rate = 3.5×10^{14} molecules s^{-1}) to a 51 nm thick hexagonal crystalline ice film at 202 K. Panel A presents the temporal profile of gas-phase HCl (m/z = 36) observed before and during exposure. Panel B shows the FTIR−RAS spectra of the reactant ice film at t = 0, 4, 10, and 15 min after opening the butterfly valve.

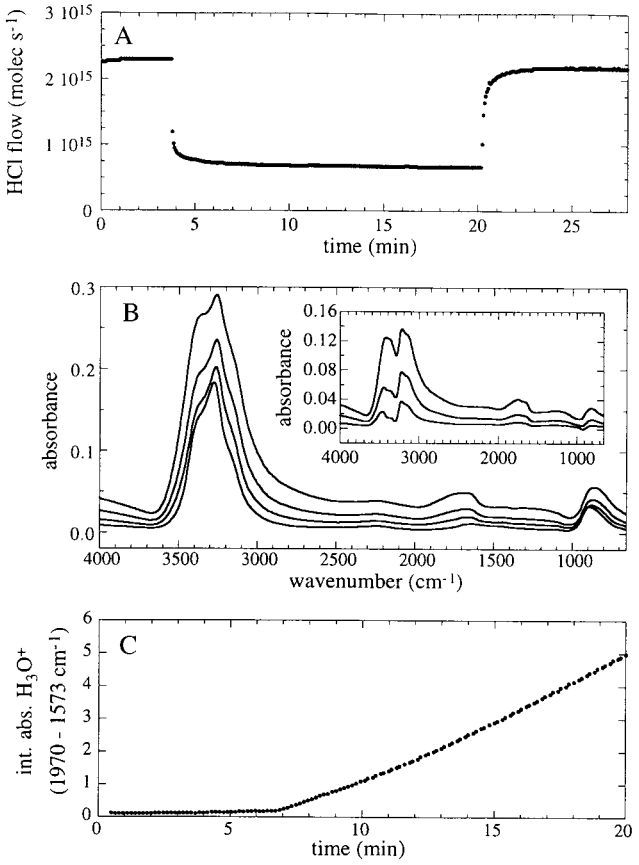

Figure 7. Infrared spectra and mass spectrometer temporal profiles obtained upon the exposure of a high HCl flow rate (flow rate = 2.3×10^{15} molecules s^{-1}) to a 20 nm thick hexagonal crystalline ice film at 202 K. Panel A shows the temporal profile of HCl (m/z = 36) observed by the mass spectrometer. Panel B shows the changes observed in the FTIR−RAS spectra of the reactant ice film at t = 0, 3.2, 5.8, and 9.9 min after opening the butterfly valve. Subtraction spectra at these times are given in the inset of panel B to highlight changes which were observed in the condensed phase. Panel C shows a temporal profile of the H_3O^+ reaction product (1970−1573 cm^{-1}) observed prior to and during exposure.

(H_3O^+). However, due to the large increase in light extinction from surface roughening an unambiguous identification of this absorbance as due to H_3O^+ product formation is not possible.

Experiments identical to that detailed above were performed at 202 K for HCl flow rates of 5.7×10^{13}, 4.0×10^{14}, and 5.7×10^{14} molecules s^{-1}. In each case, similar temporal behavior was observed in the condensed and gas phases. Specifically, when the butterfly valve was opened a large drop was observed followed by a slow recovery on a time scale ranging 30−60 min. In each case, very few changes in the infrared spectra of the reactant ice film were noted other than a net increase in light scattering from the film.

In contrast to the results outlined above, upon exposing a reactant ice film to larger HCl flow rates ($\geq 2.3 \times 10^{15}$ molecules s^{-1}) at 202 K vastly different behavior was observed in both gas and condensed phases. As an example, Figure 7A shows a m/z = 36 temporal profile for a HCl flow of 2.3×10^{15} molecules s^{-1} interacting with a ≈20 nm thick crystalline ice film at 202 K. Upon opening the butterfly valve the mass spectrometer signals rapidly dropped and no recovery was observed for reaction times up to 60 min. Upon closing the butterfly valve, the mass spectrometer signals rapidly recovered to their values prior to exposure. Opening the butterfly valve a second time resulted in identical decreases in the mass spectrometer signals at m/z = 36 and 35. Using eq II, the mass spectrometer signals yield an average reaction efficiency of 0.005. Identical experiments were conducted at HCl flows of 2.8×10^{15} and 4.6×10^{15} molecules s^{-1}. These experiments were also characterized by a large decrease in m/z 36 and 35 with no noticeable recovery observable over 60 min of exposure time.

Accompanying the outlined changes in gas-phase composition, rapid changes in the condensed-phase spectra of the reactant ice film were observed upon HCl exposure at high flow rates ($\geq 2.3 \times 10^{15}$ molecules s^{-1}) at 202 K. Figure 7B shows the infrared spectra prior to and during the exposure of a 20 nm ice film to a flow of 2.3×10^{15} HCl molecules s^{-1} at 202 K. Subtraction spectra are shown in the inset of Figure 7B to emphasize the rapid changes which were observed. The spectra shown in Figure 7B indicate a loss of intensity in the OH stretching mode (3280 cm^{-1}) and libration (850 cm^{-1}) of crystalline ice, in addition to the growth of several broad absorption features centered at 1750, 1220, and 785 cm^{-1}. In addition, the growth of a broad absorption feature centered at 3400 cm^{-1} can be inferred by taking into consideration the simultaneous decrease in intensity at 3280 cm^{-1} due to loss of the reactant ice film. The appearance and growth of new absorption features can be attributed to the O−H stretching frequency (3400 cm^{-1}), ν_4 (1750 cm^{-1}) asymmetric bend, ν_2

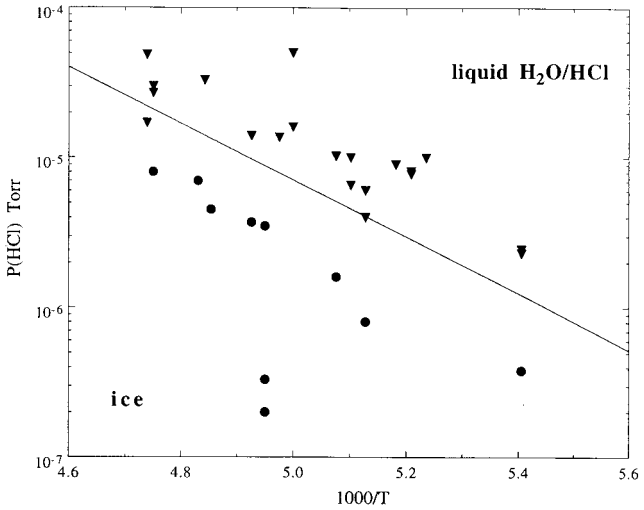

Figure 8. Summary of the experimental conditions used in the present study of HCl + ice over a range of atmospherically relevant temperatures. Partial pressures of HCl immediately after opening the butterfly valve are plotted versus $1/T$. The ice/liquid (HCl/H_2O) coexistence line determined by Abbatt et al. is also plotted.[17] The symbol ▼ signifies experimental conditions in which continuous uptake was observed in both the gas and condensed-phase probes, and ● represents experimental conditions in which time-dependent uptake was observed in the mass spectrometer temporal profiles. As shown in the plot and discussed in the text, deposition conditions in which P_{HCl} was above the coexistence line resulted in unlimited uptake while all experiments below resulted in near monolayer uptake.

(1220 cm^{-1}) symmetric bend, and torsion (785 cm^{-1}) of H_3O^+ arising from the formation of an amorphous H_2O/HCl product adlayer of composition (7 ± 1):1, H_2O:HCl.[37] Thus, the condensed-phase spectra indicate that the growth of an amorphous HCl:H_2O product layer occurred simultaneously with a loss of crystalline water ice. The temporal evolution of the ν_4 (1750 cm^{-1}) asymmetric bend of H_3O^+ is presented in Figure 7C. In combination, both temporal profiles shown in Figure 7, parts A and C, suggest that the unlimited uptake observed in the gas phase accompanies continuous growth of amorphous HCl:H_2O adlayers. Under conditions of HCl flows of 2.8×10^{15} and 4.6×10^{15} molecules s^{-1} the formation and growth of amorphous H_2O/HCl mixtures on crystalline ice at 202 K was also observed. Further, the acquired product spectra displayed evidence for the formation of more concentrated amorphous HCl/H_2O layers at higher HCl flows. This was observed as an increase in the relative intensity of the H_3O^+ absorption at 1750 cm^{-1} compared to the OH absorptions at 3400 cm^{-1}.

The uptake of HCl on ice was investigated over the temperature range of 185 to 210 K. For all temperatures investigated two uptake regimes, time-dependent and unlimited, were noted and characterized as a function of HCl flow rate into the chamber. The film thickness of our reactant ice films was varied over the range of 10−100 nm with no effect on the observed temporal behavior. The experimental conditions investigated are summarized in Figure 8. The threshold HCl flow rate between time-dependent and unlimited uptake regimes was observed to increase with increasing temperature. In addition, unlimited uptake was always observed simultaneously with the formation of amorphous H_2O/HCl product adlayers of varying composition dependent on the HCl flow into the chamber. An explanation of this behavior in the context of the HCl/H_2O phase diagram follows in the discussion section.

HBr and HI on Ice at 185−210 K. The reactivity of HBr and HI with thin crystalline water ice films was also studied over a range of stratospherically and tropospherically relevant temperatures (185−210 K). In these experiments HBr and HI flows over the range $(500-1.5) \times 10^{13}$ molecules s^{-1} were exposed to ice films varying from 10 to 100 nm in thickness.

Figures 9A and 10A show $m/z = 80$ (HBr^+) and $m/z = 128$ (HI^+) temporal profiles obtained upon exposing flows of 1.9×10^{15} and 1.0×10^{14} molecules s^{-1} of HBr and HI, respectively, to 38(HBr) and 10(HI) nm thick crystalline ice films at 185 K. Upon opening the butterfly valve rapid decreases in mass spectrometer signals ($m/z = 79$, 80, 81, 82 and $m/z = 127$ and 128) were observed. The mass spectrometer signals remained constant for the entire duration that the butterfly valve was opened and rapidly recovered upon closing the butterfly valve. Opening the butterfly valve a second time resulted in identical temporal behavior. Using eq II, the mass spectrometer signals ($m/z = 80$ and $m/z = 128$) before and after opening the butterfly valve yield reaction efficiencies of $\gamma = 0.02$ for both experiments. Uptake coefficients larger than this value cannot be measured by the current apparatus due to the substrate dimensions and background partial pressures of HBr and HI in the mass spectrometer. Therefore, we report lower limits of $\gamma \geq 0.02$ for reactions 5 and 6. The uptake of HI and HBr was investigated over a range of temperatures (185−210 K), and in all cases exposure resulted in unlimited uptake with $\gamma \geq 0.02$.

In the condensed phase, uptake of HBr and HI initiated rapid changes in the FTIR−RAS spectra of the reactant crystalline ice film. Figures 9B and 10B show the FTIR−RAS spectra of crystalline ice films prior to and during exposure to flows of HBr and HI, respectively. The structured decreases in intensity at $\nu = 3260$ cm^{-1} and $\nu = 850$ cm^{-1} can be attributed to the loss of lattice-bound H_2O in crystalline water ice. In addition to these changes, the subtraction spectra (shown in the inset) also indicate the appearance and growth of amorphous HBr/H_2O and HI/H_2O product adlayers which may be inferred from the appearance and growth of absorption features centered at 1750, 1220, and 771 cm^{-1}. The growth of the broad absorption feature centered at 3400 cm^{-1}, characteristic of HX/H_2O amorphous mixtures, can be also inferred by taking into consideration the simultaneous decrease in intensity at 3280 cm^{-1} due to loss of the reactant ice film. The temporal behavior of the condensed-phase H_3O^+ product is shown in Figures 9C and 10C. These figures clearly show that exposure of HBr and HI to ice resulted in continuous uptake at a constant rate. As expected, the composition of the product layers varied with the flow of HBr and HI exposed to the ice film. At higher HBr and HI flow rates, more concentrated amorphous HX/H_2O mixtures formed. In addition, the rate of product adlayer formation increased linearly with increasing HX (HBr or HI) flow rate into the chamber.

Formation of Crystalline Products. Although a variety of stable crystalline hydrates are known to exist for the HX:H_2O systems over the temperature and pressure range studied,[17,20,22,38] the direct formation of crystalline hydrogen halide hydrate product layers was never observed in the experiments described above. Nonetheless, secondary nucleation and growth of crystalline hydrate adlayers from amorphous H_2O:HX product layers were observed under certain experimental conditions. Most noteworthy, the nucleation of crystalline HBr hydrates was observed to occur readily at high HBr flow rates (flow ≥ 3.1×10^{15} molecules s^{-1}). Figure 11A shows the changes observed upon exposing a 10 nm thick crystalline ice film at 185 K to a HBr flow of 3.1×10^{15} molecules s^{-1}. Initially, changes in the infrared spectra were primarily characterized by the appearance and growth of absorption features at 3400, 1750, 1220, and 771 cm^{-1} due to the formation of an amorphous H_2O:HBr mixture

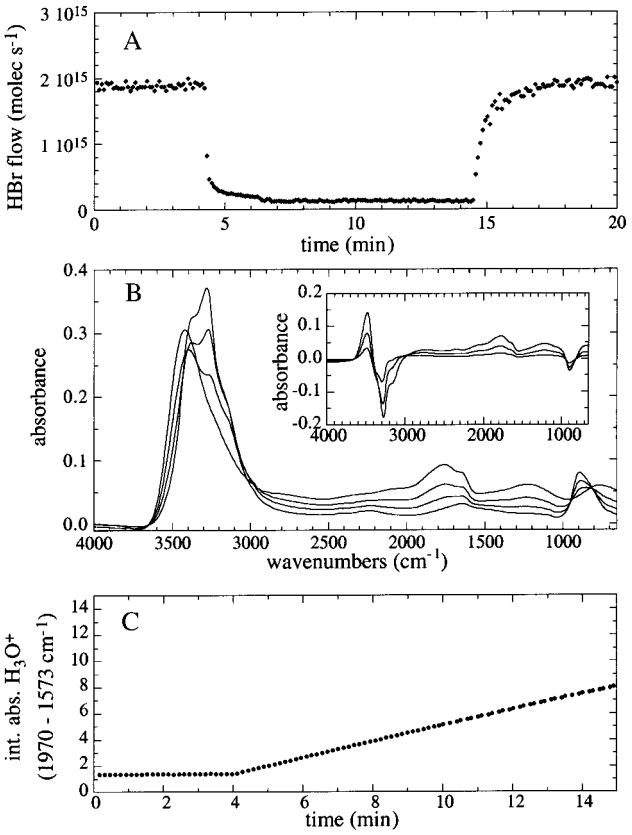

Figure 9. Infrared spectra and mass spectrometer temporal profiles obtained upon the exposure of a HBr flow (flow rate = 1.9×10^{15} molecules s^{-1}) to a 38 nm thick crystalline ice film at 185 K. Panel A shows the temporal profile of gas-phase HBr ($m/z = 80$) before and during exposure to the reactant ice film. Panel B presents the FTIR−RAS spectra acquired at $t = 0$, 3.35, 7.00, and 13.20 min after exposure of an equivalent flow. Subtraction spectra are presented to highlight the changes which occurred in the condensed phase upon exposure. Panel C shows the integrated area of the H_3O^+ product (1970−1573 cm^{-1}) as a function of exposure time.

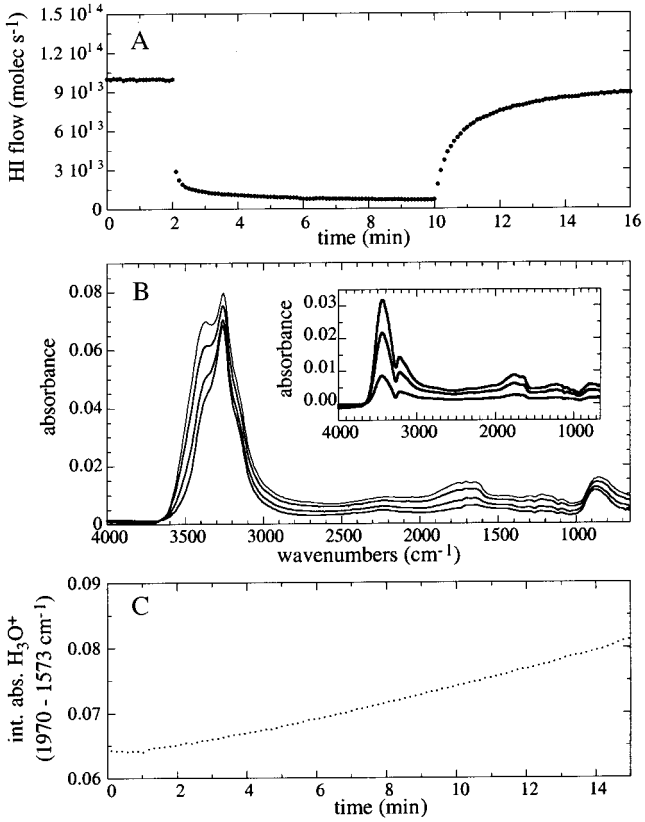

Figure 10. Infrared spectra and mass spectrometer temporal profiles obtained upon the exposure of a HI flow (flow rate = 1.0×10^{14} molecules s^{-1}) to a 10 nm thick crystalline ice film at 185 K. Panel A presents the temporal profile of gas-phase HI ($m/z = 128$) as observed by the mass spectrometer prior to and during exposure. Panel B shows the infrared spectra of the reactant film at $t = 0$, 5.35, 11.47, and 16.52 min after exposure of a similar flow. An inset is provided in Panel B which shows subtraction spectra acquired for the times above. Panel C presents a temporal profile of the condensed phase H_3O^+ absorption peak (1970−1573 cm^{-1}) observed upon opening the butterfly valve.

on the ice surface. However, at approximately $t = 10$ min, dramatic changes in the condensed-phase spectra occurred. These changes are most likely attributed to the nucleation of a new crystalline phase out of the amorphous HBr:H_2O surface layer. The onset of nucleation and growth of a crystalline HBr/H_2O product layer can be inferred from the appearance of sharp absorption features throughout the entire mid-IR range of our detector. A spectrum is shown in Figure 11B resulting from the subtraction of spectra taken at times 7.4 and 20.4 min to highlight the appearance of new peaks at 3366, 3329, 3001, 2062, 1846, 1704, 1249, 1212, 840, 765, and 698 cm^{-1}. A comparison of the subtraction spectra shown Figure 11B with the reference spectra presented in Figure 2B suggests that at high HBr flow rates (flow $\geq 3.1 \times 10^{15}$ molecules s^{-1}) a mixture of trihydrate (3:1 H_2O:HBr) and tetrahydrate (4:1 H_2O:HBr) nucleated out of the amorphous HBr:H_2O surface layer initially deposited.

Discussion

Deposition of HX on Ice at 110 K. HCl and HBr were observed to react efficiently with crystalline and amorphous microporous ice at 110 K. In each case, uptake resulted in the rapid appearance of a broad absorption feature centered around 1750 cm^{-1} in the condensed-phase spectra which may be attributed to the formation of a H_3O^+ reaction product. [30,31,34,35]

This observation strongly suggests that solvation and ionization dominate the interaction of HCl and HBr with both crystalline and amorphous microporous ice films at 110 K:

$$HCl + H_2O(s) \rightarrow H_3O^+ + Cl^- \quad (4a)$$

$$HBr + H_2O(s) \rightarrow H_3O^+ + Br^- \quad (5a)$$

In support of this reaction mechanism, a decrease in lattice-bound H_2O was observed simultaneously with the appearance of the reaction products. No evidence for adsorbed hydrogen halides in a molecular form (nondissociated) was observed in the condensed phase ice spectra for exposure time up to 60 min. We are able to characterize our sensitivity for detecting surface-absorbed HCl and HBr in their molecular (nondissociated form) by observing the spectra obtained from low-temperature deposition (94 K) on the aluminum substrate. These experiments yield an upper limit of HX (≡ HCl or HBr) $\leq 4 \times 10^{14}$ molecules cm^{-2} adsorbed on amorphous microporous and crystalline ice films in their molecular (nondissociated) form at 110 K.

Although efficiently taken up upon exposure to a clean ice film, the rates for reactions 4 and 5 decreased rapidly as a function of exposure time. This was observed as decreases in both the gas-phase HX loss rate and condensed phase H_3O^+ production rate. Together these observations suggest that reactions 4 and 5 at 110 K are initially kinetically regulated by

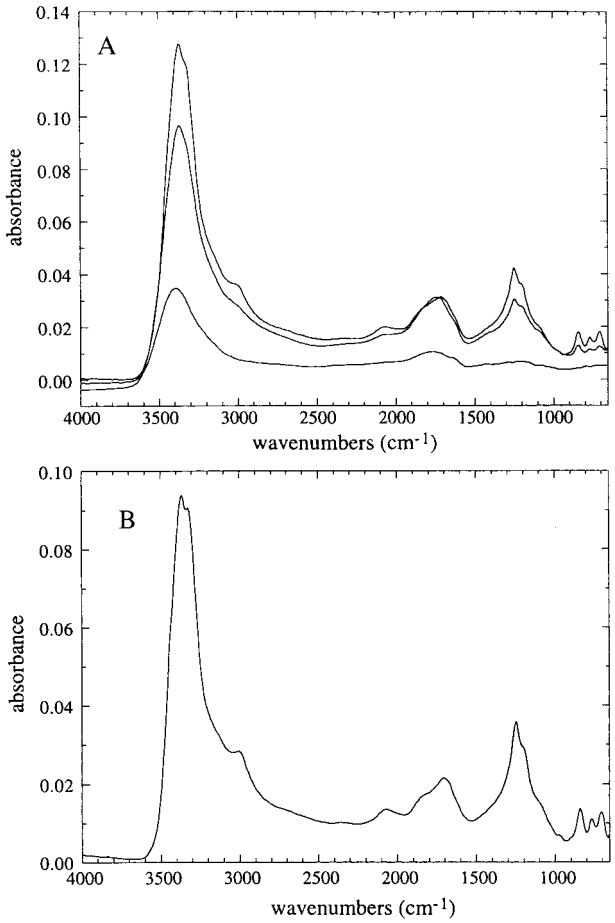

Figure 11. Infrared spectra obtained upon exposing a large HBr flow ($\geq 3.1 \times 10^{15}$ molecules s^{-1}) to a 10 nm crystalline ice film at 185 K. In panel A, spectra are shown at $t = 7.4$, 15.3, and 20.4 min. The spectra presented suggest that a crystalline phase nucleated out of a supercooled H_2O/HBr liquid adlayer. Panel B shows a spectrum obtained by subtracting the spectra at 7.4 from that at 20.4 min to highlight the new peaks observed. Comparison of the spectrum in panel B with the reference spectra in Figure 2B suggests that a mixture of the trihydrate and tetrahydrate was formed from HBr deposition on ice at high flow rates.

the availability of reactive sites on the ice film surface. Therefore, as the reaction proceeds and the number of surface sites available for reaction is reduced, the uptake becomes less efficient. Although the rates of reactions 4 and 5 were slow at long reaction times ($\gamma \leq 4.0 \times 10^{-4}$), continual exposure eventually did lead to a complete conversion of the reactant ice film to an amorphous H_2O:HX mixture for the thinnest films investigated. This temporal behavior suggests that once surface saturation occurs, uptake is regulated by slower processes such as diffusion across grain boundaries into the ice bulk.

By integrating the areas of the mass spectrometer temporal profiles shown in Figures 4A and 5A the total number of HX molecules lost to the ice surfaces can be obtained for each exposure. The results of such an analysis for HCl experiments are summarized in Table 2. Assuming that there are 1.15×10^{15} reaction sites cm^{-2} on a crystalline ice film and using a geometric surface area of the substrate (72 cm^2) as an estimate of the surface area of the reactant ice film, it can be concluded that uptake of HX species on crystalline ice is limited to approximately 5 monolayers prior to surface saturation. Using a similar analysis, the uptake of HCl on amorphous microporous ice is found to be approximately 10 monolayers. HBr exposure to crystalline and amorphous microporous ice films at 110 K

TABLE 2: Saturation Surface Coverages of HX on Ice (molecules cm^{-2}) from Mass Spectrometer Gas-Phase Temporal Profiles

HX	temp (K)	phase	flow rate[b] (molec s^{-1})	surface coverage (molec cm^{-2})	monolayer[a]
HCl	110	cryst	9.3×10^{14}	$(5.8 \pm 2.2) \times 10^{15}$	5.0
HCl	110	micro	8.8×10^{14}	$(1.1 \pm 0.3) \times 10^{16}$	9.6
HCl	202	cryst	3.5×10^{14}	$(3.5 \pm 1.6) \times 10^{15}$	2.3
HBr	110	cryst	1.92×10^{15}	$(1.2 \pm 0.3) \times 10^{16}$	10.8
HBr	110	micro	1.89×10^{15}	$(2.0 \pm 0.5) \times 10^{16}$	17.4

[a] Assuming 1.15×10^{15} sites per monolayer. [b] Flow rate prior to opening the butterfly valve.

yielded surface coverages greater than that observed for HCl by approximately a factor of 2 (see Table 2). This suggests that fewer water molecules are required to solvate impinging HBr molecules than HCl and thus, a greater net number of sites exist for reaction with HBr. This observation may be related to the lower bond energy of the H−X bond in HBr. Thermodynamic calculations on the interaction of HBr with ice films at lower temperature may be helpful in explaining the observed enhanced uptake of HBr at 110 K.

Supporting the enhanced reactivity of microporous ice evident in the mass spectrometer temporal profiles, the infrared product spectra also suggest that more H_3O^+ is formed from reactions 4 and 5 on microporous ice than on crystalline ice surfaces at 110 K. Using the integrated area of the 1750 cm^{-1} band as a proxy for the net amount of HX reacted, uptake of HX on microporous ice is approximately (3 ± 1) times that of crystalline ice at the time of surface saturation. Although overlapping within their respective error bars, the enhancement observed in the condensed phase is slightly larger than that inferred from the mass spectrometer temporal profiles. This deviation is likely attributable to experimental difficulties involved with measuring large reaction probabilities due to the onset of a significant pressure gradient in the system. Therefore, the uptake values presented in Table 2 for experiments on amorphous microporous ice are likely to represent lower limits.

The enhanced net reactivity of amorphous microporous ice relative to crystalline ice most likely arises from differences in the surface areas of these forms of ice. Previous work has shown that amorphous microporous ice is characterized by an abundance of holes connecting the surface and bulk.[39,25] The results of the present study suggest that at least some of the surface-bound H_2O molecules located in the micropores of ice are available for reaction with impinging hydrogen halides. In addition to loss of lattice-bound H_2O, the subtraction spectra in Figure 5B show that the free OH groups found in microporous ice, observable at 3695 cm^{-1}, completely disappear after exposure to HCl and HBr. This suggests that such free OH groups are highly reactive to the hydrogen halides studied.

Previous FTIR−RAS studies have reported similar reactivity of HCl toward crystalline water ice at low temperatures.[30,40] Banham et al. report that exposure of HCl to ice between the temperatures 80 and 150 K results in the formation of an amorphous HCl/H_2O mixture.[30] Banham et al. also observed a saturation of ice under these conditions; however, the spectra presented suggest that this resulted from a complete conversion of the entire ice film to an amorphous HCl/H_2O mixture rather than a deactivation of the surface. In the present study, for all flow conditions investigated a rapid decrease in the rate of HX incorporation to amorphous microporous and crystalline ice occurred prior to complete conversion of the ice film to an amorphous HX/H_2O mixture. However, a slow uptake ($\gamma \leq$

0.0004) of hydrogen halides was indeed observed at long times which eventually resulted in complete conversion of the thinnest ice films to amorphous HX:H_2O mixtures for the longest exposure times employed ($t > 1$ h).

Graham and Roberts performed an extensive study of the interaction of HCl with thin amorphous and crystalline ice films using temperature program desorption methods.[41,42] It should be pointed out that at the temperatures studied by Graham and Roberts ice micropores are thermodynamically unstable and rapidly collapse.[25] Graham and Roberts reported that the uptake of HCl on amorphous and crystalline ice films at 120 K results in the formation of a crystalline HCl·$6H_2O$ hydrate layer. Although the HCl product adlayers observed in the present study are hydrated in nature, an inspection of the absorption features leads to an assignment of an amorphous HCl/H_2O product layer. In support of this observation, the formation of a crystalline 6:1 H_2O/HCl hydrate from a solution is expected to be kinetically unfavorable at temperatures below the glass point temperature of $T \approx 135$ K.[43]

Graham and Roberts also reported an increase in the net reactivity of amorphous ice over that of crystalline ice surfaces in agreement with the present study. The authors argue that the enhancement was not related to changes in surface area but rather reflected a larger absorption probability of HCl on amorphous ice. In the present study the mass spectrometer temporal profiles and FTIR−RAS condensed-phase spectra clearly show an enhanced reactivity of amorphous microporous ice over that of crystalline ice. Although the onset of recovery for reaction on microporous ice occurs at later times, the observed rate of recovery was nearly identical for amorphous and crystalline ice films exposed to identical flows of HCl. To investigate the physical origin of the enhanced reactivity of amorphous microporous ice observed in the present study, the recoveries in the mass spectrometer temporal profiles shown in Figures 4A and 5A were fit to an exponential function (flow rate $= A + B \exp\{ C * t\}$). The recovery shown in Figure 4A was easily fit by an exponential function for times $\geq$8.8 min and yielded a time constant of $C = (9.47 \pm 0.15) \times 10^{-3}$ min^{-1}. Similarly, the recovery shown in Figure 5A was fit for times greater than 18.5 min and yielded a time constant of $C = (9.36 \pm 0.80) \times 10^{-3}$ min^{-1}. Within uncertainties the observed rate of recovery was the same for amorphous and crystalline ice films exposed to nearly identical flows of HCl. Therefore, our data suggests that the enhanced reactivity observed in the present study more likely results from differences in the number of reaction sites on amorphous microporous ice and crystalline ice films rather than differences in the absorption probabilities of HCl on ice. Differences in surface morphology related to the presence of micropores in the amorphous microporous ice films may explain the apparently larger number of reaction centers available for reaction with HCl with this form of ice. Finally, Graham and Roberts also reported the formation of an α-HCl layer on the surface of the HCl/H_2O product layer that is attributed to surface absorption of molecular HCl. In the present study no evidence for the formation of a molecular HCl product layer was found at 110 K on either amorphous microporous or crystalline ice.

There have been far fewer previous studies of the interaction of other hydrogen halides with microporous and crystalline ice at lower temperatures. Delzeit et al. showed that co-deposition of a 1:1 mixture of HBr and H_2O on a cadmium telluride substrate between 15 and 85 K led to the formation of an amorphous HBr:H_2O mixture.[37] Peil et al. also observed amorphous HBr/H_2O formation from deposition of HBr on thin ice films at a slightly higher temperature of 90 K.[44] In agreement with both past investigations, the present studies are consistent with solvation and dissociation of HBr deposited on the surface of crystalline and microporous ice at 110 K.

HCl + Ice at 185−210 K. The uptake of HCl was studied over a range of temperatures (185−210 K), HCl flow rates (5−1000 $\times 10^{13}$ molecules s^{-1}) and ice thicknesses (10−100 nm). HCl uptake was characterized by two different temporal behaviors dependent upon the flow rate of HCl for a given temperature. At low flow rates gas-phase uptake was characterized by efficient uptake at very short reaction times followed by time-dependent uptake decreasing in magnitude at longer reaction times. An integration of the temporal profile given in Figure 6A yields a total of 3.5×10^{15} HCl molecules cm^{-2} lost to the surface during reaction. Assuming that there are 1.15×10^{15} sites cm^{-2}, this yields an estimate of 2.3 monolayers deposited during the contact time with the ice surface. Similar surface coverages were obtained for experiments with lower HCl flow rates over the range of temperatures studied and ice film thicknesses studies. Previous measurements of HCl coverages on crystalline ice range from 0.4 to 16 monolayers under stratospheric conditions ($T = 185-200$ K).[17−20,45] The wide variation in reported HCl coverages has been previously attributed to different degrees of roughness in the ice films investigated. Indeed, at $T \geq 185$ K the surface of ice is highly dynamic, thus, it is possible that during the course of our experiments the reactant ice surface was substantially roughened. Considering the wide variation in reported coverages and long ice exposure times employed in the present study, our results are in reasonable agreement with previous studies.

An identification of the condensed-phase products of reaction 4 for low HCl flow rates at 185−210 K was not possible due to the increase in scattering observed upon exposure to HCl. This increase in scattering severely impeded attempts to identify any changes due to product formation in the condensed phase. However, the observed increase in light scattering may suggest that HCl incorporation into crystalline ice leads to disruption of the ice lattice at reaction temperatures between 185 and 210 K. Similar surface roughening upon exposure of HCl has been observed in previous studies of crystalline ice.[20]

At higher flow rates of HCl, efficient and unlimited uptake was observed over the range of temperatures investigated (185−210 K). Unlimited gas-phase uptake is suggestive of the formation of HCl/H_2O product multilayers. Indeed, condensed-phase spectra always showed the production of amorphous HCl/H_2O adlayers coincident with unlimited gas-phase loss. Although FTIR−RAS cannot distinguish between the spectra of solid and liquid amorphous films, the amorphous films observed in the present study are likely to consist of either liquid HCl/H_2O solutions or supercooled HCl/H_2O amorphous mixtures depending on the experimental conditions (P_{HCl} and temperature) employed**.** Previous studies have shown that metastable supercooled liquid HCl:H_2O solutions form readily under the experimental conditions examined and can persist for long times.[38] Temporal profiles of condensed-phase H_3O^+ exhibited a constant growth rate for a given flow rate of HCl into the chamber. The condensed-phase rate of product formation was found to be directly proportional to the HCl flow rate into the chamber. Together these observations point to a mechanism of surface adlayer growth via a flux of both HCl and H_2O to the ice surface to form a liquid solution or amorphous supercooled mixture. Such a mechanism results in a continual replenishing of reaction sites (H_2O) available for reaction and therefore results in an unlimited uptake at a constant rate.

To better understand the two types of behavior observed in the present experiment it is useful to view our results in the context of the HCl/H_2O phase diagram. To aid in this interpretation, a summary of the experimental results is shown graphically in Figure 8. The HCl partial pressures immediately following the opening of the butterfly valve for each experiment are plotted in Figure 8 to most accurately represent the relevant experimental parameters. Also included in Figure 8 is the water ice−HCl/H_2O liquid coexistence line as measured by Abbatt et al.[17] It should be noted that Abbatt et al. report individual HCl partial pressures over the temperature range of 210−180 K, thus, the line drawn in Figure 8 represents the best fit ($P_{HCl} = 1.30 \times 10^{-7} * 1.65 \times 10^5 \exp(-4.81 \times 1000/T)$) to the reported values by approximating the relationship as an exponential function. An examination of Figure 8 reveals that unlimited uptake of HCl was observed for all experiments in which P_{HCl} is above the coexistence line while time-dependent uptake occurs at HCl partial pressures below this line. Also supporting this interpretation, the composition of the HCl/H_2O product layers for experiments with P_{HCl} on the coexistence line varied in composition as expected. For example the product spectra for $T = 202$ K and at the ice frost point ($P_{H_2O} = 1.68 \times 10^{-3}$ Torr) can be attributed to a H_2O/HCl solution of composition ≈7:1 (H_2O/HCl) in good agreement with the composition predicted from the phase diagram presented by Hanson and Mauersberger.[38]

The magnitude of the reaction efficiency for experiments in which HCl/H_2O liquid multilayers formed was observed to increase as a function of HCl flow rate for experiments in which γ was in our measurable range ($0.02 \geq \gamma \geq 0.0001$). Rather than being attributed to kinetic factors, the variation in γ_{obs} more likely reflects the composition of product adlayer formed in reaction 4. The pressure of HCl in the chamber rapidly collapsed to a value close to the vapor pressure of the HCl/H_2O liquid solution formed upon exposure to the reactant ice surface. Thus, the γ calculated primarily reflects the difference between the HCl partial pressure initially exposed to the reactant ice film and the equilibrium HCl vapor pressure of the product film formed. These observations provide further evidence that unlimited uptake occurs via a mechanism involving formation of a HCl/H_2O solution at the ice surface.

Uptake of HBr and HI at $T = 185-210$ K. The reaction efficiencies of HBr and HI on crystalline ice were observed to exceed the limit of our measurable values, $\gamma \geq 0.02$, and showed no temporal dependence for exposure times up to 60 min. These observations were independent of HBr (or HI) flow rate ranging from (500 to 1.5) $\times 10^{13}$ molecules s^{-1} and reactant ice temperature (185−210 K). We attribute this behavior to the efficient formation of H_2O/HBr (or HI) product multilayer layers. Indeed, the FTIR−RAS product spectra clearly show that exposure of HBr and HI to ice surfaces always initiated the formation and growth of amorphous HBr/H_2O and HI/H_2O product layers. No absorption attributable to HBr or HI in their molecular forms was observed for the entire range of experimental conditions investigated. As in the case of reaction 4, we believe that the amorphous product layers observed upon deposition of HBr and HI are likely composed of HX/H_2O liquid solutions or supercooled liquid mixtures. Therefore, we conclude that HBr and HI exist primarily in an ionized or solvated state upon reaction with ice under our experimental conditions. Unfortunately, the vapor pressures of HBr and HI over the liquid layer could not be measured due to the onset of a large pressure gradient between the mass spectrometer and reaction surface for reactions with $\gamma \geq 0.02$. Therefore, identification of the exact nature of the amorphous adlayer product (stable liquid or super cooled liquid) by comparison with the phase diagrams cannot be made. As shown in Figures 9C and 10C, the growth rate of the product layer was observed to be constant throughout the entire period of exposure and varied proportionately with HBr (and HI) flow rate into the chamber. Similar to the case of reaction 4 at high HCl flow rates, we believe that the unlimited uptake observed for reactions 5 and 6 reflects the formation of a stable adlayer containing HBr (or HI) in addition to water. In this mechanism, the flux of gas-phase H_2O to the condensed phase acts to replenish "active" water sites for reaction with the impinging hydrogen halide molecules.

Previous investigations of the interaction of HBr with thin ice films have also observed efficient and unlimited uptake.[16,21,22,46] Hanson and Ravishankara report unlimited uptake of HBr onto ice at 200 K and give a lower limit on the reaction efficiency of reaction 5 of $\gamma > 0.2$.[46] The authors attribute the efficient and unlimited uptake to the formation of a liquid H_2O/HBr product. Since the original experiments by Hanson and Ravishankara, Abbatt[16] and Chu and Heron [22] have also studied reaction 5 and confirm most of the conclusions of the original study. However, recently Chu and Heron provided evidence for the formation of an HBr/H_2O crystalline trihydrate product formed in reaction 5 in contrast to the original suggestions of Hanson and Ravishankara.[22] The evidence for hydrate formation consists of a desorption peak observed approximately 55 min after HBr exposure ($P_{HBr} = 1.0 \times 10^{-6}$ Torr) to a crystalline ice surface. We believe that the observations of Chu and Heron may be consistent with the initial formation of a liquid adlayer product from which the crystalline phase H_2O/HBr trihydrate nucleated. Chu and Heron report that in all cases crystallization of an $HBr:H_2O$ hydrate layer was observed only after significant HBr deposition ($(1.1-770) \times 10^{14}$ molecules cm^{-2}) to the ice surface. In addition, the authors note that the desorption signal indicating crystallization was most pronounced after exposure to higher partial pressures of HBr ($P_{HBr} > 4 \times 10^{-7}$ Torr). From classical nucleation theory, nucleation of a crystalline $HBr:H_2O$ phase from a liquid solution is expected to depend on both volume and composition of the liquid layer from which it forms.[47] Larger HBr surface fluxes are likely to have lead to the formation of a more concentrated and thicker liquid layers which may have facilitated the nucleation of a new crystalline phase. In the present studies, nucleation of a crystalline product from a growing $HBr:H_2O$ liquid product layer (3−4:1 H_2O:HBr) deposited onto an ice surface was only observed for experiments with HBr flow rates $\geq 3.1 \times 10^{15}$ molecules s^{-1}. A comparison of the reference spectra obtained for the crystalline HBr/H_2O hydrates and the product spectra shown in Figure 11B suggests that the crystalline HBr/H_2O product layer was composed of a mixture of trihydrate and tetrahydrates. This assignment agrees reasonably with the experimental observations and theoretical calculations of Chu and Heron.[22]

Chu and Chu also investigated the uptake of HI on crystalline ice surfaces at 188 and 195 K using flow tube kinetic techniques.[23] Similar to the results of the present study, they report that exposure of HI to thin ice films resulted in efficient and continuous uptake. A comparison of the rates of uptake between the present study and that of Chu and Chu is not possible because they only report the surface coverages observed. However, Chu and Chu provide evidence for the nucleation of a crystalline 2:1 H_2O:HI product adlayer after deposition ranging from $(1-140) \times 10^{14}$ HI molecules cm^{-2}. In contrast, the product layers observed in the present study

were amorphous in nature and crystallization was never observed. The reason for such a discrepancy is unknown but may be related to differences in experimental conditions employed in both studies such as water vapor partial pressure, HI deposition rates, and substrates employed.

Atmospheric Implications. We have shown that HCl, HBr, and HI are rapidly taken up by ice, and thus the potential for important stratospheric and tropospheric heterogeneous chemistry involving these species is very high. HCl uptake by ice in the stratosphere and upper troposphere will be limited to approximately one monolayer because HCl partial pressures in these regions fall below those corresponding to the HCl/H_2O liquid/water-ice equilibrium conditions. However, it is important to note that the predicted surface coverages for ice particles in these regions will depend not only on the HCl abundance and reaction efficiency but also on the ice surface area densities encountered. This is particularly important in the case of heterogeneous chemistry on upper tropospheric cirrus clouds in which ice surface area densities can vary by several orders of magnitude (cirrus cloud surface area densities = (20−20000) $\mu m^2\ cm^{-3}$).[24] For example, we outline two simplified limiting cases for HCl surface coverages assuming a mixing ratio of HCl of 100 pptv at 300 mb and 210 K.[13] For a cirrus cloud surface area density of $A = 20\ \mu m^2\ cm^{-3}$, the number of sites on the ice particles is 4.5 times less than the HCl molecules available for reaction. Assuming $\gamma = 0.3$ initially[48] and then decreases proportionally as fraction of reaction sites available, the ice will be coated in a monolayer of HCl in ≈16 min and gas-phase HCl partial pressures should be essentially unperturbed. Under these conditions the full monolayer HCl coverage on the ice surface would be available for reaction and chlorine activation via reaction 1 is expected to be efficient (assuming one monolayer = 1.15×10^{15} molecules cm^{-2}). In the other limiting case in which $A = 20\,000\ \mu m^2\ cm^{-3}$, the number of ice reaction sites exceeds the number of gas-phase HCl molecules available by a factor of 223. In this scenario the ice will never be fully coated with HCl and hence, subsequent reaction with $ClONO_2$ may be hampered by the availability of surface-bound HCl. Although this is a simplified picture of the ice in the atmosphere which does not take into account the ice growth or evaporation, the photochemical production of HCl, or any heterogeneous loss mechanisms of HCl, the calculations above do illustrate that the microphysical parameters of tropospheric ice will have a strong bearing on the heterogeneous chemistry of the troposphere.

Although the uptake of HBr and HI was found to be unlimited and efficient ($\gamma \geq 0.02$), it should be noted that the partial pressures used in the present study were ≈100−1000 times greater than those observed in the atmosphere.[8,49−51] Thus, it is possible that under the low pressure conditions of the atmosphere the uptake will be qualitatively different. However, because the partial pressures of HBr and HI observed in the atmosphere are very low it is unlikely that ice particles could accumulate high enough surface concentrations to form product multilayers. This is especially true given the very large surface area densities of water ice encountered in upper tropospheric cirrus clouds. For example, assuming an HBr mixing ratio of 2.0 pptv at 300 mb and 220 K, uptake onto a cirrus cloud with a surface area density of 20 $\mu m^2\ cm^{-3}$ would result in a maximum surface coverage of 0.09 of a monolayer (assuming one monolayer = 1.15×10^{15} molecules cm^{-2}).[49,50] The gas-phase abundance of HI is expected to be at least an order of magnitude lower than that of HBr,[8] therefore, HI is likely to accumulate onto tropospheric ice surfaces to an even lower extent.

The efficient incorporation of HBr and HI into atmospheric ice and snow may have important implications with respect to their mechanisms of transport and removal from the atmosphere. In the upper troposphere, the primary gas-phase loss processes of HBr and HI is currently thought to be reaction with OH radical.[7,52] Because these species are readily lost to the surface of ice, uptake onto atmospheric ice and snow followed by deposition is likely to constitute an efficient heterogeneous removal mechanism competitive with loss in the gas phase. On the other hand, uptake followed by evaporation of the ice cloud would constitute a temporary reservoir of HBr and HI and may be important in the transport of halogen species in the troposphere. Due to the highly reactive nature of HBr and HI on ice surfaces, changes in the removal rates and transport of these compounds may be important in determining their net effect on the gas phase of ozone chemistry. Therefore, modeled abundances of hydrogen halide concentrations must take into consideration not just the nucleation of ice and snow but ultimately the fate of the ice particles undergoing reaction.

Acknowledgment. The authors thank A. R. Ravishankara and R. Bianco for helpful discussions in addition to M. Robinson and T. Onasch for work on the instrument design and construction. M.A.T. gratefully acknowledges support as an NSF Young Instigator. M.A.Z. acknowledges support by a NASA Earth System Science Fellowship. This research was funded by NSF Grant ATM9711969 and NASA Grant SA98-0005.

References and Notes

(1) Farman, J. C.; Gardner, B. G.; Shanklin, J. D. *Nature* **1985**, *315*, 207.
(2) Tolbert, M. A.; Rossi, M. J.; Malhotra, R.; Goldan, D. M. *Science* **1987**, *238*, 1258−1260.
(3) Solomon, S. *Nature* **1990**, *347*, 347−354.
(4) Fahey, D. W.; Kawa, S. R.; Woodbridge, E. L.; Tin, P.; Wilson, J. C.; Jonsson, H. H.; Dye, J. E.; Baumgartner, D.; Borrmann, S.; Toohey, D. W.; Avallone, L. M.; Proffitt, M. H.; Margitan, J.; Loewenstein, M.; Podolske, J. R.; Salawitch, R. J.; Wofsy, S. C.; Ko, M. K. W.; Anderson, D. E.; Schoeberl, M. R.; Chan, K. R. *Nature* **1993**, *363*, 509−514.
(5) Hanson, D. R.; Ravishankara, A. R. *J. Geophys. Res.* **1991**, *96*, 5081−5090.
(6) Tie, X.; Brasseur, G. *Geophys. Res. Lett.* **1996**, *23*, 2505−2508.
(7) Lary, D. J.; Chipperfeld, M. P.; Toumi, R.; Lenton, T. *J. Geophys. Res.* **1996**, *101*, 1489−1504.
(8) Wennberg, P. O.; Brault, J. W.; Hanisco, T. F.; Salawitch, R. J.; Mount, G. *J. Geophys. Res.* **1996**, *102*, 8887−8898.
(9) Wang, P.; McCormick, M. P.; Poole, L. R.; Chu, W. P.; Yue, G. K.; Kent, G. S.; Skeens, K. M. *Atmos. Res.* **1994**, *34*, 53−83.
(10) Prabhakara, C.; Kratz, D. P.; Yoo, J.; Dalu, G.; Vernekar, A. *J. Quant. Spectrosc. Radiat. Transfer*. **1993**, *49*, 467−483.
(11) Reichardt, J.; Ansmann, A.; Serwazi, M.; Weitkamp, C.; Michaelis, W. *Geophys. Res. Lett.* **1996**, *23*, 1929−1932.
(12) Borrmann, S.; Solomon, S.; Dye, J. E.; Luo, B. *Geophys. Res. Lett.* **1996**, *23*, 2133−2136.
(13) Solomon, S.; Borrmann, S.; Garcia, R. R.; Portmann, R.; Thomason, L.; Poole, L. R.; Winker, D.; McCormick, M. P. *J. Geophys. Res.* **1997**, *102*, 21411−21429.
(14) Barrie, L. A.; Bottenheim, J. W.; Schnell, R. C.; Crutzen, P. J.; Rasmussen, R. A. *Nature* **1988**, *334*, 138.
(15) McConnell, J. C.; Henderson, G. S.; Barrie, L.; Bottenheim, J.; Niki, H.; Langford, C. H.; Templeton, M. *Nature* **1992**, *355*, 150.
(16) Abbatt, J. P. D. *Geophys. Res. Lett.* **1994**, *21*, 665.
(17) Abbatt, J. P. D.; Beyer, K. D.; Fucaloro, A. F.; McMahon, J. R.; Wooldridge, P. J.; Zhang, R.; Molina, M. J. *J. Geophys. Res.* **1992**, *97*, 15819.
(18) Hanson, D. R.; Ravishankara, A. R. *J. Phys. Chem.* **1992**, *96*, 2682−2691.
(19) Chu, L. T.; Leu, M.-T.; Keyser, L. F. *J. Phys. Chem.* **1993**, *97*, 7779.
(20) Foster, K. L.; Tolbert, M. A.; George, S. M. *J. Phys. Chem. A* **1997**, *101*, 4979−4986.
(21) Hanson, D. R.; Ravishankara, A. R. *J. Phys. Chem.* **1992**, *96*, 9441−9446.
(22) Chu, L. T.; Heron, J. W. *Geophys. Res. Lett.* **1995**, *22*, 3211.

(23) Chu, L. T.; Chu, L. *J. Phys. Chem. B.* **1997**, *101*, 6271−6275.

(24) Toon, O. B. International Workshop on Modeling Heterogeneous Chemistry of the Lower Stratosphere/Upper Troposphere, 1996, Bischoffsheim, France.

(25) Zondlo, M. A.; Onasch, T. B.; Tolbert, M. A.; Mallick, G.; Arentz, P.; Robinson, M. S. *J. Phys. Chem. B* **1997**, *101*, 10887.

(26) Barone, S. B.; Zondlo, M. A.; Tolbert, M. A. *J. Phys. Chem. A* **1997**, *101*, 8643.

(27) Zondlo, M. A.; Barone, S. B.; Tolbert, M. A. Reaction of $CLONO_2$, N_2O_5 and HNO_3 on ice under stratospheric conditions. XVIII Quadrennial Ozone Symposium, 1996, L'Aquila, Italy.

(28) Zondlo, M. A.; Barone, S. B.; Tolbert, M. A. *J. Phys. Chem. A* **1998**, *102*, 5736−5748.

(29) Marti, J.; Mauersberger, K. *Geophys. Res. Lett.* **1993**, *20*, 363−366.

(30) Banham, S. F.; Sodeau, J. R.; Horn, A. B.; McCoustra, M. R. S.; Chesters, M. A. *J. Vac. Sci. Technol.* **1996**, *A 14* (3), 1620−1626.

(31) Feriso, C. C.; Hornig, D. F. *J. Chem. Phys.* **1955**, *23*, 1464.

(32) Sodeau, J. R.; Horn, A. B.; Banham, S. F.; Koch, T. G. *J. Phys. Chem.* **1995**, *99*, 6258.

(33) Rowland, B.; Fisher, M.; Devlin, J. P. *J. Phys. Chem.* **1993**, *97*, 2485−2487.

(34) Gilbert, A. S.; Sheppard, N. *J. Chem. Soc., Faraday Trans.* **1973**, *69*, 1628−1642.

(35) Ritzhaupt, G. D.; Devlin, J. P. *J. Phys. Chem.* **1991**, *95*, 90−95.

(36) Brown, D. E.; George, S. M. *J. Phys. Chem.* **1996**, *100*, 15460−15469.

(37) Delzeit, L.; Rowland, B.; Devlin, J. P. *J. Phys. Chem.* **1993**, *97*, 10312−10318.

(38) Hanson, D. R.; Mauersberger, K. *J. Phys. Chem.* **1990**, *94*, 4700−4705.

(39) Berland, B.; Brown, S.; Tolbert, M. A.; George, S. M. *Geophys. Res. Lett.* **1995**, *22*, 3493−3496.

(40) Horn, A. B.; Chesters, M. A.; McCoustra, M. R. S.; Sodeau, J. R. *Chem. Soc. Faraday Trans.* **1992**, *88*, 1077−1078.

(41) Graham, J. D.; Roberts, J. T. *J. Phys. Chem.* **1994**, *98*, 5974−5983.

(42) Graham, J. D.; Roberts, J. T. *Geophys. Res. Lett.* **1995**, *22*, 251−254.

(43) Ji, K. Etude de la composition des aerosols stratospheriques polaires au moyn des diagrammes de phase stables, metastables et cinetiques des systems: HNO_3/H_2O, HCl/H_2O et H_2SO_4/H_2O, Univeresite de Paris, 1994.

(44) Peil, S.; Seisel, S.; Schrems, O. *J. Mol. Struct.* **1995**, *348*, 449−452.

(45) Domine, F.; Thibert, E.; Chaix, L. *Chemical exchange between the atmosphere and polar snow*; Springer-verlag: New York, 1996; Vol. 143.

(46) Hanson, D. R.; Ravishankara, A. R. Reactions of halogen species on ice surfaces. In *Global Environmental Change*; Springer-verlag: New York, 1993; Vol. 7, pp 281−290.

(47) Pruppacher, H. R.; Klett, J. D. *Microphysics of Clouds and Precipitation*; Kluwer Academic Publishers: Dordrecht, The Netherlands, 1985.

(48) DeMore, W. B.; Sander, S. P.; Golden, D. M.; Hampson, R. F.; Kurylo, M. J.; Howard, C. J.; Ravishankara, A. R.; Kolb, C. E.; Molina, M. J. *Chemical Kinetics and Photochemical Data for use in Stratospheric Modeling*; Jet Propulsion Laboratory, 1994.

(49) Carlotti, M.; Ade, P. A. R.; Carli, B.; Ciarpallini, P.; Cortesi, U.; Griffin, M. J.; Lepri, G.; Mencaraglia, F.; Murray, A. G.; Nolt, I. G.; Park, J. H.; Radostitz, J. V. *Geophys. Res. Lett.* **1995**, *22*, 3207−3210.

(50) Nolt, I. G.; Ade, P. A. R.; Alboni, F.; Carli, B.; Carlotti, M.; Cortesi, U.; Epifani, M.; Griffin, M. J.; Hamilton, P. A.; Lee, C.; Lepri, G.; Mencaraglia, F.; Murray, A. G.; Park, J. H.; Park, K.; Rapollini, P.; Ridolfi, M.; Vanek, M. D. *Geophys. Res. Lett.* **1997**, *24*, 281−284.

(51) Pundt, I.; Pommereau, J. P.; Phillips, C.; Lateltin, E. *J. Atmos. Chem.* **1998**, *30*, 173−185.

(52) Solomon, S.; Garcia, R. R.; Ravishankara, A. R. *J. Geophys. Res.* **1994**, *99*, 20,491−20,499.